

1 **Seeing and touching the mycomembrane at the nanoscale**

2

3 Albertus Viljoen,^{1,¶} Esther R ath,^{2,3,¶} John D. Mckinney,^{4,*} Georg E. Fantner,^{2,3,*} Yves F.
4 Dufr ne^{1,5,*}

5

6 ¹Louvain Institute of Biomolecular Science and Technology, UCLouvain, Croix du Sud, 4-5, bte L7.07.07,
7 B-1348 Louvain-la-Neuve, Belgium

8 ²Laboratory for Bio- and Nano-Instrumentation, Swiss Federal Institute of Technology Lausanne (EPFL),
9 1015 Lausanne, Switzerland

10 ³School of Engineering, Swiss Federal Institute of Technology (EPFL), 1015 Lausanne, Switzerland

11 ⁴School of Life Sciences, Swiss Federal Institute of Technology (EPFL), 1015 Lausanne, Switzerland

12 ⁵Walloon Excellence in Life sciences and Biotechnology (WELBIO), B-1300 Wavre, Belgium

13

14 * Corresponding authors:

15 yves.dufrene@uclouvain.be

16 georg.fantner@epfl.ch

17 john.mckinney@epfl.ch

18

19 [¶]Albertus Viljoen and Esther R ath contributed equally to this work. Author order was determined by
20 drawing straws.

21

22 **Short title:** Mycobacterial cell wall at the nanoscale

23 **KEYWORDS:** mycobacterial envelope, ultrastructure, adhesins, binding force, chemical properties,
24 growth dynamics, drugs, atomic force microscopy

25

26 **Author contributions (only for submission)**

27 AV, ER, JDM, GEF and YFD wrote the manuscript. JDM, GEF and YFD supervised the work.

28 **Competing interests**

29 The authors have declared that no competing interests exist.

30

31 **Abstract**

32 Mycobacteria have unique cell envelopes, surface properties and growth dynamics, which all play a part
33 in the ability of these important pathogens to infect, evade host immunity, disseminate and to resist
34 antibiotic challenges. Recent atomic force microscopy (AFM) studies have brought new insights into the
35 nanometre-scale ultrastructural and mechanical properties of mycobacteria. The molecular forces with
36 which mycobacterial adhesins bind to host factors, like heparin and fibronectin, and the hydrophobic
37 properties of the mycomembrane have been unravelled by AFM force spectroscopy studies. Real-time
38 correlative AFM and fluorescence imaging have delineated a complex interplay between surface
39 ultrastructure, tensile stresses within the cell envelope and cellular processes leading to division. The
40 unique capabilities of AFM, which include sub-diffraction limit topographic imaging and piconewton
41 force sensitivity, have great potential to resolve important questions that remain unanswered on the
42 molecular interactions, surface properties and growth dynamics of this important class of pathogens.

43

44 **The mycomembrane: from the cell surface to growth dynamics**

45 Mycobacteria owe their pathogenicity and recalcitrance to antibiotics largely to their unique cell
46 envelope (1). The mycobacterial cell envelope consists of a peptidoglycan (PG) layer bearing similarity to
47 the PG of *Escherichia coli*, with a few minor differences (2). Distinctive to the Corynebacteriaceae family,
48 from which the *Mycobacterium* genus stems, the PG is covalently linked to another large polysaccharide
49 called arabinogalactan (AG). The ends of the arabinan portion of the AG are esterified with very large
50 fatty acids (60 – 90 carbon chains) called mycolic acids forming the inner leaflet of the mycobacterial
51 outer membrane, known as the mycomembrane. The outer leaflet of the mycomembrane consists of a
52 large panoply of exotic, extractable lipids, some of them also containing mycolic acids. The
53 mycomembrane, with its densely packed large fatty acids, is thus a consequential hydrophobic barrier to
54 antibiotics and chemotherapeutic agents whose targets are periplasmic or cytosolic (1). Moreover, like
55 the PG layer, the AG and mycolic acid layers are also essential to the survival and growth of all
56 mycobacteria and therefore the biosynthetic machinery of their components are excellent drug targets
57 (viz. the antitubercular ethambutol targets AG synthesis and isoniazid and ethionamide target mycolic
58 acid synthesis).

59 The mycomembrane largely determines the physical and chemical properties of the
60 mycobacterial cell surface, a structure that is at the interface between mycobacteria and their
61 environment. Therefore the physiology and mechanics of this structure fundamentally forms a part of
62 the bigger picture of mycobacterial pathophysiology. It is on the surface of the bacteria where
63 hydrophobic lipids are exposed that drive their association with small water droplets allowing their
64 transmission by aerosols (3–5). It is also here where a large variety of lipids and saccharides interact with
65 receptors on immune cells, where specialized adhesins bind to host extracellular matrix proteins (6–8)
66 and where interbacterial interactions lead to the formation of mycobacterial cords (9, 10). New

67 evidence even suggests that features in the ultrastructure of the mycobacterial cell surface predict
68 growth and division events (11).

69 Not only is the structure of the mycobacterial cell envelope non-canonical, but the way it is
70 synthesized during growth is also very different from model rod-shaped bacteria like *E. coli* and *Bacillus*
71 *subtilis*, where new cell wall material is continuously inserted along the growing sidewalls of the cells
72 (12). In mycobacteria, insertion of new cell wall material occurs mainly at the poles (13). In addition,
73 asymmetric mycobacterial division and elongation underlies the occurrence of nascent cells with
74 variable cell lengths, a factor that contributes to single-cell phenotypic heterogeneity (14).
75 Mycobacteria, like other bacteria, rely on this phenotypic heterogeneity at the single cell level to
76 optimize survival of sub-populations of cells in diverse, often hostile microenvironments (for recent
77 review on this topic see (15)).

78 Large questions regarding the surface properties of the mycomembrane include: how strong are
79 the interactions between surface components like hydrophobic groups or adhesins and their binding
80 partners; what are the nanoscale distributions of these components on the surface; how does the
81 ultrastructure of the mycobacterial surface change as the bacteria grow and divide; and how is
82 phenotypic heterogeneity reflected in the ultrastructural and biophysical properties of the cells at the
83 nanoscale? As a single cell-technique with sub-diffraction limit resolution and force sensitivity, atomic
84 force microscopy (AFM) has helped to address these questions.

85 **AFM: Feeling The Force**

86 AFM functions by touching samples with a very sharp tip (probe) using a small force (e.g. 100
87 pN), while raster scanning to obtain topographic images with x - y resolution that can range from ~50 nm
88 on cells to less than a nanometer on model membranes (16). Different imaging modes of AFM exist,
89 including correlative imaging with fluorescence microscopy (Fig. 1A), and gentle, fast and dynamic

90 modes allowing real-time visualization of single proteins performing their actions and undergoing
91 conformational changes in 2D crystals or in supported lipid bilayers (for more details see (17–19)). But
92 AFM is also an ultrasensitive force measuring device, an approach called force spectroscopy (Fig. 1B)
93 (20). Here force-distance curves are recorded by pushing the tip against the sample and then retracting
94 it while monitoring force and the exact position of the tip at each point of its movement, enabling the
95 investigation of physical properties and molecular interactions. These include cell wall mechanics
96 (stiffness/ elasticity/ tensile strength), surface hydrophobicity and the binding strength between
97 receptors and their ligands. Furthermore, recording arrays of force-distance curves across the surface
98 allows spatial mapping of these properties with nanoscale resolution (21, 22).

99 **Functional Analysis Of Single Adhesins**

100 Bacterial pathogenesis is often initiated by the interaction between bacterial adhesins and
101 specific ligands on the host cell surface (Fig. 2A). In the context of tuberculosis, evidence from *ex vivo*
102 studies indicate that inhaled *Mycobacterium tuberculosis* bacilli adhere to epithelial cells lining alveoli, in
103 a step that possibly precedes the infection of their preferred, but less abundant, macrophage host cells
104 (23–26). At more advanced stages of disease, the bacilli disseminate into the host lymphatic system and
105 bloodstream (27). In this process, the bacteria are exposed to physical shear forces, which they resist by
106 adhering to extracellular matrix proteins (28). A variety of adhesins were identified that contribute to
107 the ability of mycobacteria to bind to abiotic surfaces or to host extracellular matrix proteins (7, 8, 25,
108 26, 29). Pertinent questions are (i) how strong are the interactions between adhesins and their ligands
109 and (ii) what is the nanoscale distribution of the adhesins on the bacterial surface? AFM single molecule
110 force spectroscopy (SMFS) has proven a valuable tool to answer these questions. SMFS consists of using
111 AFM tips modified with ligands to probe their cognate receptors (Fig. 2B) enabling the quantification of
112 the molecular forces in these interactions and mapping the distribution of the receptors (e.g. single
113 adhesins) on the surface of living bacteria (30).

114 The *M. tuberculosis* heparin-binding hemagglutinin (HBHA) surface adhesin works as a
115 multifunctional adhesin. The C-terminal heparin-binding domain containing several lysine-rich repeats,
116 binds to heparan sulphate proteoglycan (HSPG) receptors on target epithelial cells (6, 31, 32), but HBHA
117 can also form homodimers or homopolymers *via* an α -helical coiled-coil region in the N-terminus of the
118 protein (31). In addition, it was found that HBHA-coated latex beads could cross epithelial cell layers *via*
119 transcytosis, which involved the reorganization of actin filaments in these cells (33). However, the
120 strength and molecular mechanism of binding in these interactions were not unravelled. In a pioneering
121 AFM study, the forces driving the interaction between HBHA and heparin sulphate proteoglycan (HSPG)
122 receptors were captured by SMFS (34). AFM tips modified with single HBHA molecules were used to
123 probe model surfaces coated with heparin, revealing that single electrostatic ($\text{lysine}^+\text{-SO}_4^-$)
124 intermolecular bridges between the two binding partners resisted relatively weak forces of ~ 50 pN. The
125 data also showed that multiple such bridges form with increased contact time, strengthening the HBHA-
126 heparin interaction, suggesting that clustering of HBHA on the bacterial cell surface may drive strong
127 adhesion. Indeed, AFM tips modified with heparin molecules could probe interactions with HBHA on
128 living mycobacterial cells (Fig. 2A), allowing mapping of their nanoscale localization and revealing that
129 the adhesins clustered within nanodomains on the bacterial surface. This phenomenon may favor the
130 recruitment of proteoglycan receptors within lipid rafts (35). A similar approach using HBHA-modified
131 tips revealed a homogenous distribution of HSPG receptors on living pneumocytes (37). Interestingly,
132 when the AFM tip was retracted at high speeds (high pulling velocities), force curve signatures were
133 observed that are typical for the extraction of plasma membrane tethers, structures that may play a role
134 in host cell invasion. When it comes to homophilic interactions, SMFS unveiled a bimodal force
135 distribution (~ 70 and 130 pN) for HBHA-HBHA interactions indicating the participation of multimers in
136 the coiled-coil-dependent interaction (36). AFM SMFS studies also demonstrated the involvement of
137 both C-terminal and N-terminal domains of HBHA in its interaction with actin (37). Another question

138 that AFM studies helped to address about HBHA regarding its surface localization despite the absence of
139 a signal peptide directing its secretion *via* traditional protein secretion systems. SMFS with heparin-
140 functionalized probes demonstrated a sharp decrease in detection of the HBHA-heparin force signature
141 on *Mycobacterium smegmatis* cells lacking its orthologue of the putative preprotein translocase
142 Rv0613c (38). Taken together HBHA served as an excellent platform to explore how AFM SMFS studies
143 could be applied to mycobacterial adhesins to reveal the forces whereby they interact with their ligands,
144 to explore their interaction with different ligands and to map the locations of adhesins on the
145 mycobacterial surface at the nanoscale.

146 Mycobacteria also employ adhesins that specifically bind to extracellular matrix proteins, such
147 as fibronectin (Fn) (39–41). The interaction between Fn and Fn-binding proteins (FnBPs) in *M. bovis* BCG
148 has also been investigated by SMFS (42, 43). Force mapping revealed a homogenous distribution of
149 FnBPs on the surfaces of these mycobacteria, which was altered by treatment with polysaccharide-
150 degrading enzymes or AG-targeting ethambutol, indicating that the major mycobacterial FnBPs are
151 associated with the mycomembrane and not anchored to the plasma membrane. Although the major
152 specific mycobacterial FnBP was not identified in this study, prime candidates are the Fn attachment
153 protein (Fap) encoded by *Rv1860* that was originally identified in *Mycobacterium avium* (44) and the
154 multifunctional Antigen 85 (Ag85) complex (40). All members of the Ag85 complex possess a highly
155 conserved and unique-to-mycobacteria Fn-binding sequence (40, 45, 46). In the multidrug resistant,
156 emerging, nontuberculous pathogen *Mycobacterium abscessus* a single Fap orthologue shows poor
157 conservation of the sequences necessary for Fn binding, while four Ag85 orthologues are present with
158 highly conserved Fn-binding domains (45, 47). *M. abscessus* could thus be used to study the Ag85-Fn
159 specific interaction by SMFS (48). Blocking experiments with peptides containing specific binding site
160 sequences of either Fn or Ag85 demonstrated specificity of the interaction and that the Ag85 complex
161 counts for the major Fn-binding activity in this mycobacterium. Notably, it was observed that the Ag85-

162 Fn specific interaction appeared to be mechanically activated with a sharp increase in binding forces
163 from ~75 pN at low pulling speeds to ~500 pN at greater speeds. Moreover, modelling of the force-
164 loading rate dependency using Friddle-Noy-de Yoreo theory (49) allowed calculation of thermodynamic
165 parameters of the interaction, including the dissociation constant. The strong bonds observed under
166 high tensile loading may favor strong mycobacterial attachment in the lung where cells are exposed to
167 high shear stress or during hematogenous spread leading to a disseminated infection (28). Single-
168 molecule experiments might soon reveal more stress-sensitive adhesins among mycobacteria. In the
169 same line molecular recognition experiments may be used to study the interactions between host cell
170 receptors, such as lectins and their mycobacterial lipid ligands.

171 **Cell envelope lipids define hydrophobic and hydrophilic cell-surface nanodomains**

172 Hydrophobic forces are involved in many molecular processes, such as protein folding,
173 membrane fusion and cell adhesion. In pathogenesis, they often favor the adhesion of the bacteria to
174 surfaces and tissues (50). In mycobacteria, the cell surface is rich in hydrophobic mycolic acids, therefore
175 assessing this property is an important issue (Fig. 2A). While the hydrophobic nature of the
176 mycobacterial cell envelope is highly documented, the hydrophobicity of single mycobacterial cells and
177 in particular the distribution of hydrophobic groups on their surfaces has been under explored. In this
178 regard, AFM force spectroscopy with hydrophobic tips has proved to be a valuable method to measure
179 local hydrophobic forces on living mycobacteria (51, 52). In the case of *M. bovis* BCG, a uniform and,
180 unsurprisingly, very hydrophobic cell surface was observed that corresponded with force measurements
181 made on model substrates coated with self-assembled monolayers of alkanethiols exposing hydrophobic
182 methyl groups (52, 53). Notably, treatment of cells with antitubercular drugs that inhibit the synthesis of
183 mycolic acids (isoniazid) or AG (ethambutol) resulted in sharp decreases in hydrophobic adhesive forces
184 measured on some cells. On other cells hydrophilic nanodomains appeared, likely because of the loss of
185 outer layers of the mycomembrane exposing a deeper (PG) hydrophilic layer (51, 53). These results

186 indicate that the hydrophobic character of mycobacterial cells is conferred by mycolic acids exposed on
187 their surfaces.

188 Several nontuberculous mycobacteria, including the pathogens *M. avium* and *M. abscessus*
189 produce large quantities of a class of surface-exposed polar lipids (less hydrophobic than mycolic acids)
190 known as glycopeptidolipids (GPLs) (54). In *M. abscessus*, the irreversible transition from a GPL⁺ to GPL⁻
191 phenotype directly correlates with a clinically important change from a smooth to a rough colony
192 morphotype (54). The rough variant tends to grow as cords of bacteria tightly packed against each other,
193 a physical arrangement that protects them from the host immune system and antimicrobials, making
194 infections with this variant severe and very challenging to treat (55–57). On the other hand, GPLs appear
195 to be necessary for optimal biofilm formation and play immunomodulatory roles that may be important
196 during early stages of infection (58–60). Recently, newly developed multiparametric AFM imaging with
197 improved spatial resolution revealed striking hydrophobic and hydrophilic nanodomains that were only
198 present on a GPL⁺-*M. abscessus* strain (Fig. 2B) (61). Hydrophilic nanodomains may thus represent areas
199 in which more polar GPL classes are concentrated, while hydrophobic nanodomains mainly contain
200 more apolar GPLs and/or mycolic acids. Such partitioning of surface lipids suggests a role for the spatial
201 variation of hydrophobic properties in adhesion and biofilm formation. With GPLs masking pro-
202 inflammatory lipid factors while being highly immunogenic themselves (62–64), nanodomains enriched
203 in GPLs (or certain classes of GPLs) or in which GPLs are more sparse may also play a role in antigen
204 presentation. Importantly, the compound BM212 that inhibits the essential mycolic acid flippase
205 induced a sharp reduction in surface hydrophobicity of both smooth and rough variants (61),
206 highlighting along with the earlier work done on *M. bovis* BCG, the antiadhesive activity of
207 antituberculars that target mycolic acid synthesis or transport (51, 53).

208 **Effect Of Antibiotics On The Mycomembrane**

209 The combination of AFM with antibiotic treatments represents a valuable approach to decipher
210 the very complex architecture of the mycobacterial cell wall, and may help us understand how structural
211 alterations of the wall lead to cell death. Initial investigations of mycobacterial surfaces revealed smooth
212 surfaces (52, 65). However, treatment with both cell-wall active drugs (isoniazid, ethionamide and
213 ethambutol) and an antibiotic targeting protein translation (streptomycin) led to alterations on *M. bovis*
214 BCG surfaces increasing their roughness (51). In the case of ethambutol that targets AG specifically (Fig.
215 3A), concentric striations were observed at its minimal inhibitory concentration (MIC), while at
216 concentrations above the MIC an additional perpendicular layer also exhibiting concentric striations
217 became apparent (65). These different layers may be partially synthesized and, hence, non-esterified AG
218 and underlying PG, respectively. This view is supported by the fact that surface alterations were
219 accompanied by a dramatic loss of surface hydrophobicity probably due to the loss of the mycolic-acid
220 rich mycomembrane (51). The functional consequences of AG inhibition by ethambutol and isoniazid on
221 cell wall nanomechanics were investigated in real-time (66). Both antitubercular drugs led to sharp
222 decreases in cell wall stiffness and elasticity, which showed different time-dependencies. Interestingly,
223 the nanomechanical effect of ethambutol was cell cycle dependent (67), with cells at different division
224 phases showing different responses to the drug. More recently, it was found that in the absence of L,D-
225 transpeptidase activity responsible for the non-canonical 3-3 cross-links that are abundant in
226 mycobacterial PG, the bacteria exhibited alterations in cell wall stiffness and were more sensitive to
227 drugs inhibiting the enzymes responsible for canonical 4-3 cross-links (68).

228 Focusing on deeper layers of the mycobacterial cell envelope, immunogold AFM imaging of
229 ethambutol- or isoniazid-treated *M. bovis* BCG detected and localized lipoarabinomannan (LAM) on the
230 surfaces of these cells but not on the surfaces of untreated cells (51). SMFS studies utilizing anti-LAM
231 antibody-functionalized AFM tips later confirmed these results (69). Molecular mapping of LAM on
232 untreated *M. bovis* BCG cells showed that LAM was present at very low levels on these cell surfaces (< 5

233 % binding frequency). On isoniazid-treated cells, anti-LAM-LAM interactions occurred at a high
234 frequency and force maps revealed that LAM clustered into nanodomains in these cells, probably
235 reflecting areas in which the mycomembrane had been disrupted.

236 Considering differences in the lipid compositions and antibiotic susceptibilities between
237 different mycobacterial species, in particular between tubercle bacilli and non-tuberculous
238 mycobacteria, future AFM studies are warranted to delineate the ultrastructural changes that occur on
239 the bacterial cell surfaces under exposure to different classes of antibiotics.

240 **Cell Growth Dynamics**

241 Cell growth and subsequent cell division are two essential phases of proliferation for all bacterial
242 species. The macromolecular mechanisms underlying growth and division in mycobacteria are different
243 from other bacterial genera (70). Bacterial cell growth is accomplished by localized peptidoglycan
244 synthesis at distinct regions such as the septum (*Staphylococcus aureus*), the lateral cell wall (*Bacillus*
245 *subtilis*, *Escherichia coli*) or the poles (*Mycobacterium species*) (12, 71). Studying the polar growth at
246 subdiffractional level revealed that the site of growth is guided by the tropomyosin-like protein
247 DivIVA/Wag31, which is located at the cell tip, whereas the enzymes for cell wall biogenesis are located
248 subpolarly (72). Mycobacterial cell elongation and division lead to daughter cells of different sizes (14,
249 73–75), which gives rise to population heterogeneity. This heterogeneity may be beneficial for the
250 survival in the host and under antibiotic pressure (14, 70, 76). There has been a controversy on the
251 pattern of mycobacterial single-cell growth. While a unipolar growth model proposes that cells elongate
252 preferentially at the old pole between cell birth and division (14), a bipolar model suggests that both
253 poles elongate at equal rates during the period between cell separation and cytokinesis with a
254 subsequent predominant growth of the old pole (74). Recently, it was shown that mycobacterial cell
255 growth neither follows a unipolar nor a bipolar pattern. Instead, a biphasic growth model for the new

256 pole was proposed based on time-lapse correlative AFM-optical microscopy (Fig. 3A) imaging of
257 *Mycobacterium smegmatis*, and confirmed on other pathogenic species (*Mycobacterium tuberculosis*,
258 *Mycobacterium abscessus*, *Mycobacterium marinum*) using optical microscopy (77). The authors
259 observed a rate-change transition of the newly born pole from a slow- to a fast-growing state with a
260 delay of variable time length (“new end take off” – NETO), whereas the old pole shows a fast and
261 constant growth (Fig. 3B). This rate-change occurs mostly before cell division, but can also occur after
262 cell division. Therefore, the authors conclude that NETO and the event of cell division are not linked.
263 Instead, the degree of growth asymmetry at cell division depends on the difference between NETO-
264 delay and interdivision time. By using the AFM tip as a nanomanipulator to lyse or remove the
265 neighboring sibling cell, they showed that the pre-NETO time is not caused by physical constraints (Fig.
266 3B). In order to investigate whether the delay before NETO is associated with a delayed relocalization of
267 the molecules required for cell wall biogenesis, the authors studied the localization of DivIVA/Wag31.
268 They observed a partial relocalization of DivIVA/Wag31 from the old to the new poles during the pre-
269 NETO phase (77).

270 Bacterial growth is followed by cell division, which is a spatially and temporally highly
271 coordinated process (78). This process involves the selection of the time point and location of the
272 division site (79), control of synthesis, and disassembly of cell wall components at the division site,
273 while keeping integrity (80) and cell shape (12). Because mycobacteria have a complex cell wall, the
274 mechanisms underlying cell division differ from other bacterial models (78). Using high resolution
275 microscopy techniques, morphological features of the cell surface were identified and linked to the
276 inception and completion of bacterial division. Investigations with electron microscopy (scanning
277 electron microscopy and transmission electron microscopy) revealed circular division scars at the newly
278 formed poles after cell separation (81, 82). As AFM enables live-cell studies, morphological
279 characteristics during the cell separation process, including the emergence of a septal furrow prior to

280 division, could be observed in real-time (67). The ability of AFM to measure 3D profiles revealed
281 waveform troughs on the corrugated cell surface of *Mycobacterium smegmatis* (11). Employing time-
282 lapse single-cell imaging, the center-most trough near mid-cell was linked to the division site, which
283 points to the importance of wave troughs as the earliest known reference point for the future division
284 site. Long-term imaging over several generations showed that cells inherit these morphological features
285 from the (grand-)mother cell. Assembly of the FtsZ ring is localized at a pre-existing wave trough near
286 mid-cell position, as shown by correlative AFM-optical microscopy.

287 Mycobacterial cell division is coordinated by the divisome, a macromolecular complex of
288 multiple proteins, including peptidoglycan synthases and hydrolases, which assembles at the mid-cell
289 position to synthesize the septum before separation into two daughter cells (79, 83). Recent studies
290 suggest that in addition to molecular mechanisms, mechanical forces are involved during the cell
291 division process in *Staphylococcus aureus* and *Actinobacteria* (84, 85). By deploying the capability of
292 AFM to measure mechanical properties, the co-operation of localized enzymatic activity and mechanical
293 forces to separate sibling cells were identified in *Mycobacterium smegmatis* (86). Turgor pressure,
294 through a concentration of tensile stress at the pre-cleavage furrow in combination with diminished
295 material strength due to the enzymatic activity of RipA peptidoglycan hydrolase leads to fast cell
296 cleavage (Fig. 3C,D). In contrast, reducing cell wall hydrolysis by inducing decreased expression of RipA
297 inhibits cell cleavage, which results in chains of non-growing cells where only the two outermost poles
298 elongate. By using AFM as a nanomanipulation tool to apply additional force on the septum, direct cell
299 cleavage was observed even for chained RipA-depleted cells. Taken together, these AFM investigations
300 provide a detailed picture of the mycobacterial cell division in time and space (Fig 3E). After birth, the
301 cell elongates by creating new wave troughs (Fig 3E.1). Approximately 2-4h after cell birth, the FtsZ-ring
302 starts to form in the center-most wave trough (Fig 3E.2). Shortly after, a small circumferential band
303 occurs co-located with the FtsZ ring (Fig 3E.3). This pre-cleavage furrow is only a few nanometers deep.

304 The stiffness of the pre-cleavage furrow steadily increases as the cell division progresses. (Fig 3E.4).
305 Once cytokinesis is complete, Wag31 appears co-located with the pre-cleavage furrow (Fig 3B.5), and
306 the localized stress in the membrane continued to increase (Fig 3E.5). Once the stress at the pre-
307 cleavage furrow exceeds the tensile strength of the cell wall material, the bacteria separate abruptly in
308 what appears to be a turgor pressure driven fracture process (Fig 3E.6). After cell separation, the old
309 poles continue to grow at their previous growth velocity, however the new poles initially grow
310 significantly slower (Fig 3E.7). After a while, the new pole undergoes a transition in growth velocity from
311 the slow regime to the same growth velocity as the old pole (NETO), (Fig 3E.8). At this point the cycle
312 begins again.

313

314 **Conclusions**

315 In the past years, AFM studies have brought important new insights into mycobacterial
316 physiology. Nanoscale mapping of the surface of living mycobacteria with specific functionalized AFM
317 probes has enabled determination of the strength and dynamics of adhesin-ligand interactions and to
318 quantify chemical properties like surface hydrophobicity. Time-lapse imaging has contributed to our
319 understanding of mycobacterial division and growth, of surface ultrastructure and how the latter is
320 altered by cell-wall active antibiotics. What lies ahead?

321 Beyond the examples reviewed herein, huge untapped potential exists for the use of AFM
322 technologies in the study of mycobacteria: Real-time correlative and multiparametric imaging has
323 already proven its merit to correlate cellular processes with ultrastructural, chemical and mechanical
324 characteristics of the mycomembrane. While important discoveries were made relating to growth and
325 division of model mycobacteria under optimal growth conditions, the next steps would include to
326 address the nanoscale surface characteristics of clinically important mycobacteria, including
327 *Mycobacterium tuberculosis*, under conditions that are more relevant to their pathogenesis, for example
328 those that stimulate dormancy.

329 Force spectroscopy modes have been helpful to characterise the interactions between
330 mycobacterial adhesins and host factors, but the potential to combine SMFS molecular recognition with
331 topographic imaging, an approach that has delivered numerous insights into surface protein clustering
332 (87), has not been delved into for mycobacteria. Several mycobacterial proteins and lipids were
333 identified that act as adhesins binding to host factors, but these interactions remain poorly
334 characterized (7, 8). In addition to unravelling the molecular forces in the interactions between their
335 cognate ligands and mycobacterial adhesins (or surface components recognized by immune cell
336 receptors), SMFS may serve as a platform to characterize thermodynamic and kinetic parameters of

337 these interactions and may serve as an excellent tool to discover compounds with therapeutic potential.
338 Also, the potential of SCFS studies to investigate direct cell-cell interactions, for example between
339 individual mycobacterial cells or between single mycobacterial cells and single host cells has not been
340 explored. This approach has been applied with massive payoff in the investigation of cell adhesion of a
341 number of Gram-positive and negative pathogens (88).

342 Some exciting AFM technologies still need to see their first use in the study of mycobacteria.
343 High speed AFM (HS-AFM) has been used to make movies of integral membrane proteins, such as
344 transporters performing their activities in real time (18, 19, 89). HS-AFM may offer a solution for the
345 analysis of substrate transport dynamics in mycobacterial antibiotic efflux pumps and mycomembrane
346 lipid transporters, for which bioassays are scarce. Another exciting AFM technology that has yet to be
347 used with mycobacteria is fluid force microscopy (Fluid FM) (90–92), where a hollow AFM cantilever
348 (and tip) is connected to a microfluidics device allowing, for example, the collection of single bacterial
349 cells for so-called single-cell force spectroscopy (SCFS) analyses. SCFS consists of using an AFM tip (e.g. a
350 Fluid FM tip) exposing a single cell to probe a target surface, such as the surface of another bacterium or
351 a macrophage cell exposing pattern recognition receptors. Combined Fluid FM and SCFS may thus prove
352 itself incredibly useful to directly assay the forces with which different mycobacterial strains or mutants
353 (e.g. lacking surface-exposed lipids) bind host macrophage cells in the step preceding cellular invasion.

354 Many questions remain regarding the complex ultrastructure of the mycobacterial envelope,
355 which seems to vary significantly between single cells, particularly during different stages of infection
356 (2). There are also unsolved questions regarding the unique asymmetric growth dynamics of
357 mycobacteria, resulting in sister cells having distinct characteristics (13, 70). As AFM technology is
358 continuously evolving with higher speed, greater force sensitivity and stability, and higher resolution
359 (18), we are confident that many of these problems will be resolved in the next decade.

360 **Acknowledgments**

361 Work at UCLouvain was supported by the Excellence of Science-EOS programme (Grant #30550343), the
362 European Research Council (ERC) under the European Union's Horizon 2020 research and innovation
363 programme (grant agreement n°693630), the FNRS-WELBIO (grant n°WELBIO-CR-2015A-05), the
364 National Fund for Scientific Research (FNRS), and the Research Department of the Communauté
365 française de Belgique (Concerted Research Action). Work at EPFL was supported by the ERC through
366 CoG-773091 : InCell to GEF, and the Swiss National Science Foundation through grant 200021_182562 to
367 GEF, and through grants 310030B_176397 and IZLSZ3_170912 to JDM. Y.F.D. is Research Director at the
368 FNRS. The funders had no role in study design, data collection and analysis, decision to publish, or
369 preparation of the manuscript.

370

371 **REFERENCES**

372

- 373 1. Jarlier V, Nikaido H. 1994. Mycobacterial cell wall: structure and role in natural resistance to
374 antibiotics. *FEMS Microbiol Lett* 123:11–18.
- 375 2. Dulberger CL, Rubin EJ, Boutte CC. 2020. The mycobacterial cell envelope - a moving target. *Nat*
376 *Rev Microbiol* 18:47–59.
- 377 3. Falkinham JO. 2003. Mycobacterial Aerosols and Respiratory Disease. *Emerg Infect Dis* 9:763–767.
- 378 4. Cambier CJ, Falkow S, Ramakrishnan L. 2014. Host evasion and exploitation schemes of
379 *Mycobacterium tuberculosis*. *Cell* 159:1497–1509.
- 380 5. Jankute M, Nataraj V, Lee OY-C, Wu HHT, Ridell M, Garton NJ, Barer MR, Minnikin DE, Bhatt A,
381 Besra GS. 2017. The role of hydrophobicity in tuberculosis evolution and pathogenicity. *Sci Rep*
382 7:1315.
- 383 6. Pethe K, Alonso S, Biet F, Delogu G, Brennan MJ, Locht C, Menozzi FD. 2001. The heparin-binding
384 haemagglutinin of *M. tuberculosis* is required for extrapulmonary dissemination. 6843. *Nature*
385 412:190–194.
- 386 7. Govender VS, Ramsugit S, Pillay M. 2014. *Mycobacterium tuberculosis* adhesins: potential
387 biomarkers as anti-tuberculosis therapeutic and diagnostic targets. *Microbiology (Reading, Engl)*
388 160:1821–1831.
- 389 8. Vinod V, Vijayrajratnam S, Vasudevan AK, Biswas R. 2020. The cell surface adhesins of
390 *Mycobacterium tuberculosis*. *Microbiological Research* 232:126392.

- 391 9. Middlebrook G, Dubos RJ, Pierce C. 1947. Virulence and morphological characteristics of
392 mammalian tubercle bacilli. *J Exp Med* 86:175–184.
- 393 10. Bloch H, Sorkin E, Erlenmeyer H. 1953. A toxic lipid component of the tubercle bacillus (cord
394 factor). I. Isolation from petroleum ether extracts of young bacterial cultures. *Am Rev Tuberc*
395 67:629–643.
- 396 11. Eskandarian HA, Odermatt PD, Ven JXY, Hannebelle MTM, Nievergelt AP, Dhar N, McKinney JD,
397 Fantner GE. 2017. Division site selection linked to inherited cell surface wave troughs in
398 mycobacteria. *Nat Microbiol* 2:17094.
- 399 12. Cabeen MT, Jacobs-Wagner C. 2005. Bacterial cell shape. *Nature Reviews Microbiology* 3:601–610.
- 400 13. Baranowski C, Rego EH, Rubin EJ. 2019. The Dream of a Mycobacterium. *Microbiol Spectr* 7.
- 401 14. Aldridge BB, Fernandez-Suarez M, Heller D, Ambravaneswaran V, Irimia D, Toner M, Fortune SM.
402 2012. Asymmetry and aging of mycobacterial cells lead to variable growth and antibiotic
403 susceptibility. *Science* 335:100–104.
- 404 15. Dhar N, McKinney J, Manina G. 2016. Phenotypic Heterogeneity in *Mycobacterium tuberculosis*.
405 *Microbiology Spectrum* 4:TBTB2-0021–2016.
- 406 16. Dufrène YF. 2008. Towards nanomicrobiology using atomic force microscopy. *Nat Rev Microbiol*
407 6:674–680.
- 408 17. Dufrène YF, Ando T, Garcia R, Alsteens D, Martinez-Martin D, Engel A, Gerber C, Müller DJ. 2017.
409 Imaging modes of atomic force microscopy for application in molecular and cell biology. *Nat*
410 *Nanotechnol* 12:295–307.

- 411 18. Ando T. 2017. High-speed atomic force microscopy and its future prospects. *Biophys Rev* 10:285–
412 292.
- 413 19. Heath GR, Scheuring S. 2019. Advances in high-speed atomic force microscopy (HS-AFM) reveal
414 dynamics of transmembrane channels and transporters. *Curr Opin Struct Biol* 57:93–102.
- 415 20. Dufrière YF, Pelling AE. 2013. Force nanoscopy of cell mechanics and cell adhesion. *Nanoscale*
416 5:4094–4104.
- 417 21. Dufrière YF, Martínez-Martín D, Medalsy I, Alsteens D, Müller DJ. 2013. Multiparametric imaging of
418 biological systems by force-distance curve-based AFM. *Nat Methods* 10:847–854.
- 419 22. Alsteens D, Müller DJ, Dufrière YF. 2017. Multiparametric Atomic Force Microscopy Imaging of
420 Biomolecular and Cellular Systems. *Acc Chem Res* 50:924–931.
- 421 23. Bermudez LE, Goodman J. 1996. *Mycobacterium tuberculosis* invades and replicates within type II
422 alveolar cells. *Infect Immun* 64:1400–1406.
- 423 24. Ashiru OT, Pillay M, Sturm AW. 2010. Adhesion to and invasion of pulmonary epithelial cells by the
424 F15/LAM4/KZN and Beijing strains of *Mycobacterium tuberculosis*. *J Med Microbiol* 59:528–533.
- 425 25. Ashiru OT, Pillay M, Sturm AW. 2012. *Mycobacterium tuberculosis* isolates grown under oxygen
426 deprivation invade pulmonary epithelial cells. *Anaerobe* 18:471–474.
- 427 26. Bhattacharya J, Westphalen K. 2016. Macrophage-epithelial interactions in pulmonary alveoli.
428 *Semin Immunopathol* 38:461–469.
- 429 27. Russell DG. 2007. Who puts the tubercle in tuberculosis? *Nat Rev Microbiol* 5:39–47.

- 430 28. Clark RA, Blakley SL, Greer D, Smith MH, Brandon W, Wisniewski TL. 1991. Hematogenous
431 dissemination of *Mycobacterium tuberculosis* in patients with AIDS. Rev Infect Dis 13:1089–1092.
- 432 29. Stokes RW, Norris-Jones R, Brooks DE, Beveridge TJ, Doxsee D, Thorson LM. 2004. The Glycan-Rich
433 Outer Layer of the Cell Wall of *Mycobacterium tuberculosis* Acts as an Antiphagocytic Capsule
434 Limiting the Association of the Bacterium with Macrophages. Infect Immun 72:5676–5686.
- 435 30. Hinterdorfer P, Dufrêne YF. 2006. Detection and localization of single molecular recognition events
436 using atomic force microscopy. Nat Methods 3:347–355.
- 437 31. Delogu G, Brennan MJ. 1999. Functional Domains Present in the Mycobacterial Hemagglutinin,
438 HBHA. J Bacteriol 181:7464–7469.
- 439 32. Pethe K, Aumercier M, Fort E, Gatot C, Locht C, Menozzi FD. 2000. Characterization of the Heparin-
440 binding Site of the Mycobacterial Heparin-binding Hemagglutinin Adhesin. J Biol Chem 275:14273–
441 14280.
- 442 33. Menozzi FD, Reddy VM, Cayet D, Raze D, Debrie A-S, Dehouck M-P, Cecchelli R, Locht C. 2006.
443 *Mycobacterium tuberculosis* heparin-binding haemagglutinin adhesin (HBHA) triggers receptor-
444 mediated transcytosis without altering the integrity of tight junctions. Microbes and Infection 8:1–
445 9.
- 446 34. Dupres V, Menozzi FD, Locht C, Clare BH, Abbott NL, Cuenot S, Bompard C, Raze D, Dufrêne YF.
447 2005. Nanoscale mapping and functional analysis of individual adhesins on living bacteria. Nat
448 Methods 2:515–520.
- 449 35. Tkachenko E, Simons M. 2002. Clustering Induces Redistribution of Syndecan-4 Core Protein into
450 Raft Membrane Domains. J Biol Chem 277:19946–19951.

- 451 36. Verbelen C, Raze D, Dewitte F, Locht C, Dufrêne YF. 2007. Single-molecule force spectroscopy of
452 mycobacterial adhesin-adhesin interactions. *J Bacteriol* 189:8801–8806.
- 453 37. Verbelen C, Dupres V, Raze D, Bompard C, Locht C, Dufrêne YF. 2008. Interaction of the
454 mycobacterial heparin-binding hemagglutinin with actin, as evidenced by single-molecule force
455 spectroscopy. *J Bacteriol* 190:7614–7620.
- 456 38. Veyron-Churlet R, Dupres V, Saliou J-M, Lafont F, Raze D, Locht C. 2018. Rv0613c/MSMEG_1285
457 Interacts with HBHA and Mediates Its Proper Cell-Surface Exposure in Mycobacteria. *Int J Mol Sci*
458 19.
- 459 39. Ratliff TL, McGarr JA, Abou-Zeid C, Rook GA, Stanford JL, Aslanzadeh J, Brown EJ. 1988. Attachment
460 of mycobacteria to fibronectin-coated surfaces. *J Gen Microbiol* 134:1307–1313.
- 461 40. Abou-Zeid C, Ratliff TL, Wiker HG, Harboe M, Bennedsen J, Rook GA. 1988. Characterization of
462 fibronectin-binding antigens released by *Mycobacterium tuberculosis* and *Mycobacterium bovis*
463 BCG. *Infect Immun* 56:3046–3051.
- 464 41. Abou-Zeid C, Garbe T, Lathigra R, Wiker HG, Harboe M, Rook GA, Young DB. 1991. Genetic and
465 immunological analysis of *Mycobacterium tuberculosis* fibronectin-binding proteins. *Infect Immun*
466 59:2712–2718.
- 467 42. Verbelen C, Dufrêne YF. 2009. Direct measurement of Mycobacterium-fibronectin interactions.
468 *Integr Biol (Camb)* 1:296–300.
- 469 43. Hall-Stoodley L, Watts G, Crowther JE, Balagopal A, Torrelles JB, Robison-Cox J, Bargatze RF,
470 Harmsen AG, Crouch EC, Schlesinger LS. 2006. *Mycobacterium tuberculosis* binding to human

- 471 surfactant proteins A and D, fibronectin, and small airway epithelial cells under shear conditions.
472 Infect Immun 74:3587–3596.
- 473 44. Schorey JS, Li Q, McCourt DW, Bong-Mastek M, Clark-Curtiss JE, Ratliff TL, Brown EJ. 1995. A
474 *Mycobacterium leprae* gene encoding a fibronectin binding protein is used for efficient invasion of
475 epithelial cells and Schwann cells. Infect Immun 63:2652–2657.
- 476 45. Naito M, Ohara N, Matsumoto S, Yamada T. 1998. The novel fibronectin-binding motif and key
477 residues of mycobacteria. J Biol Chem 273:2905–2909.
- 478 46. Kuo C-J, Bell H, Hsieh C-L, Ptak CP, Chang Y-F. 2012. Novel Mycobacteria Antigen 85 Complex
479 Binding Motif on Fibronectin. J Biol Chem 287:1892–1902.
- 480 47. Schorey JS, Holsti MA, Ratliff TL, Allen PM, Brown EJ. 1996. Characterization of the fibronectin-
481 attachment protein of *Mycobacterium avium* reveals a fibronectin-binding motif conserved among
482 mycobacteria. Molecular Microbiology 21:321–329.
- 483 48. Viljoen A, Alsteens D, Dufrêne Y. 2020. Mechanical Forces between Mycobacterial Antigen 85
484 Complex and Fibronectin. Cells 9:716.
- 485 49. Friddle RW, Noy A, Yoreo JJD. 2012. Interpreting the widespread nonlinear force spectra of
486 intermolecular bonds. PNAS 109:13573–13578.
- 487 50. Doyle RJ. 2000. Contribution of the hydrophobic effect to microbial infection. Microbes Infect
488 2:391–400.
- 489 51. Alsteens D, Verbelen C, Dague E, Raze D, Baulard AR, Dufrêne YF. 2008. Organization of the
490 mycobacterial cell wall: a nanoscale view. Pflugers Arch - Eur J Physiol 456:117–125.

- 491 52. Dague E, Alsteens D, Latgé J-P, Verbelen C, Raze D, Baulard AR, Dufrêne YF. 2007. Chemical force
492 microscopy of single live cells. *Nano Lett* 7:3026–3030.
- 493 53. Alsteens D, Dague E, Rouxhet PG, Baulard AR, Dufrêne YF. 2007. Direct measurement of
494 hydrophobic forces on cell surfaces using AFM. *Langmuir* 23:11977–11979.
- 495 54. Gutiérrez AV, Viljoen A, Ghigo E, Herrmann J-L, Kremer L. 2018. Glycopeptidolipids, a Double-
496 Edged Sword of the *Mycobacterium abscessus* Complex. *Front Microbiol* 9:1145.
- 497 55. Catherinot E, Roux A-L, Macheras E, Hubert D, Matmar M, Dannhoffer L, Chinet T, Morand P,
498 Poyart C, Heym B, Rottman M, Gaillard J-L, Herrmann J-L. 2009. Acute respiratory failure involving
499 an R variant of *Mycobacterium abscessus*. *J Clin Microbiol* 47:271–274.
- 500 56. Nessar R, Cambau E, Reytrat JM, Murray A, Gicquel B. 2012. *Mycobacterium abscessus*: a new
501 antibiotic nightmare. *J Antimicrob Chemother* 67:810–818.
- 502 57. Bernut A, Herrmann J-L, Kissa K, Dubremetz J-F, Gaillard J-L, Lutfalla G, Kremer L. 2014.
503 *Mycobacterium abscessus* cording prevents phagocytosis and promotes abscess formation. *Proc*
504 *Natl Acad Sci USA* 111:E943-952.
- 505 58. Howard ST, Rhoades E, Recht J, Pang X, Alsup A, Kolter R, Lyons CR, Byrd TF. 2006. Spontaneous
506 reversion of *Mycobacterium abscessus* from a smooth to a rough morphotype is associated with
507 reduced expression of glycopeptidolipid and reacquisition of an invasive phenotype. *Microbiology*
508 (Reading, Engl) 152:1581–1590.
- 509 59. Roux A-L, Viljoen A, Bah A, Simeone R, Bernut A, Laencina L, Deramautd T, Rottman M, Gaillard J-L,
510 Majlessi L, Brosch R, Girard-Misguich F, Vergne I, de Chastellier C, Kremer L, Herrmann J-L. 2016.

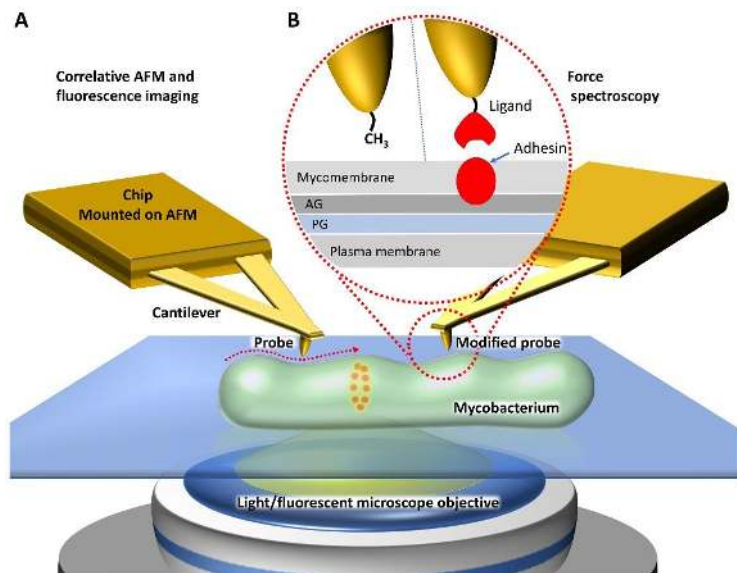
- 511 The distinct fate of smooth and rough *Mycobacterium abscessus* variants inside macrophages.
512 Open Biol 6:pii: 16018.
- 513 60. Whang J, Back YW, Lee K-I, Fujiwara N, Paik S, Choi CH, Park J-K, Kim H-J. 2017. *Mycobacterium*
514 *abscessus* glycopeptidolipids inhibit macrophage apoptosis and bacterial spreading by targeting
515 mitochondrial cyclophilin D. Cell Death Dis 8:e3012.
- 516 61. Viljoen A, Viela F, Kremer L, Dufrêne YF. 2020. Fast chemical force microscopy demonstrates that
517 glycopeptidolipids define nanodomains of varying hydrophobicity on mycobacteria. Nanoscale
518 Horiz 5:944-953.
- 519 62. Schorey JS, Sweet L. 2008. The mycobacterial glycopeptidolipids: structure, function, and their role
520 in pathogenesis. Glycobiology 18:832–841.
- 521 63. Rhoades ER, Archambault AS, Greendyke R, Hsu F-F, Streeter C, Byrd TF. 2009. *Mycobacterium*
522 *abscessus* Glycopeptidolipids Mask Underlying Cell Wall Phosphatidyl-myo-Inositol Mannosides
523 Blocking Induction of Human Macrophage TNF- α by Preventing Interaction with TLR2. The Journal
524 of Immunology 183:1997–2007.
- 525 64. Davidson LB, Nessar R, Kempaiah P, Perkins DJ, Byrd TF. 2011. *Mycobacterium abscessus*
526 Glycopeptidolipid Prevents Respiratory Epithelial TLR2 Signaling as Measured by H β D2 Gene
527 Expression and IL-8 Release. PLOS ONE 6:e29148.
- 528 65. Verbelen C, Dupres V, Menozzi FD, Raze D, Baulard AR, Hols P, Dufrêne YF. 2006. Ethambutol-
529 induced alterations in *Mycobacterium bovis* BCG imaged by atomic force microscopy. FEMS
530 Microbiol Lett 264:192–197.

- 531 66. Wu Y, Zhou A. 2009. *In situ*, real-time tracking of cell wall topography and nanomechanics of
532 antimycobacterial drugs treated *Mycobacterium JLS* using atomic force microscopy. Chem
533 Commun 7021–7023.
- 534 67. Wu Y, Sims RC, Zhou A. 2014. AFM resolves effects of ethambutol on nanomechanics and
535 nanostructures of single dividing mycobacteria in real-time. Phys Chem Chem Phys 16:19156–
536 19164.
- 537 68. Baranowski C, Welsh MA, Sham L-T, Eskandarian HA, Lim HC, Kieser KJ, Wagner JC, McKinney JD,
538 Fantner GE, Ioerger TR, Walker S, Bernhardt TG, Rubin EJ, Rego EH. 2018. Maturing *Mycobacterium*
539 *smegmatis* peptidoglycan requires non-canonical crosslinks to maintain shape. Elife 7:e37516.
- 540 69. Verbelen C, Christiaens N, Alsteens D, Dupres V, Baulard AR, Dufrêne YF. 2009. Molecular mapping
541 of lipoarabinomannans on mycobacteria. Langmuir 25:4324–4327.
- 542 70. Kieser KJ, Rubin EJ. 2014. How sisters grow apart: mycobacterial growth and division. Nat Rev
543 Microbiol 12:550–562.
- 544 71. Thanky NR, Young DB, Robertson BD. 2007. Unusual features of the cell cycle in mycobacteria:
545 polar-restricted growth and the snapping-model of cell division. Tuberculosis (Edinb) 87:231–236.
- 546 72. Meniche X, Otten R, Siegrist MS, Baer CE, Murphy KC, Bertozzi CR, Sassetti CM. 2014. Subpolar
547 addition of new cell wall is directed by DivIVA in mycobacteria. Proc Natl Acad Sci USA 111:E3243-
548 3251.
- 549 73. Joyce G, Williams KJ, Robb M, Noens E, Tizzano B, Shahrezaei V, Robertson BD. 2012. Cell Division
550 Site Placement and Asymmetric Growth in Mycobacteria. PLoS One 7:e44582.

- 551 74. Santi I, Dhar N, Bousbaine D, Wakamoto Y, McKinney JD. 2013. Single-cell dynamics of the
552 chromosome replication and cell division cycles in mycobacteria. *Nature Communications* 4:2470.
- 553 75. Singh B, Nitharwal RG, Ramesh M, Pettersson BMF, Kirsebom LA, Dasgupta S. 2013. Asymmetric
554 growth and division in *Mycobacterium* spp.: compensatory mechanisms for non-medial septa.
555 *Molecular Microbiology* 88:64–76.
- 556 76. Rego EH, Audette RE, Rubin EJ. 2017. Deletion of a mycobacterial divisome factor collapses single-
557 cell phenotypic heterogeneity. *Nature* 546:153–157.
- 558 77. Hannebelle MTM, Ven JXY, Toniolo C, Eskandarian HA, Vuaridel-Thurre G, McKinney JD, Fantner
559 GE. 2020. A biphasic growth model for cell pole elongation in mycobacteria. *Nature*
560 *Communications* 11:452.
- 561 78. Hett EC, Rubin EJ. 2008. Bacterial Growth and Cell Division: a Mycobacterial Perspective. *Microbiol*
562 *Mol Biol Rev* 72:126–156.
- 563 79. Egan AJF, Vollmer W. 2013. The physiology of bacterial cell division. *Annals of the New York*
564 *Academy of Sciences* 1277:8–28.
- 565 80. Chao MC, Kieser KJ, Minami S, Mavrici D, Aldridge BB, Fortune SM, Alber T, Rubin EJ. 2013. Protein
566 complexes and proteolytic activation of the cell wall hydrolase RipA regulate septal resolution in
567 mycobacteria. *PLoS Pathog* 9:e1003197.
- 568 81. Takade A, Takeya K, Taniguchi H, Mizuguchi Y. 1983. Electron microscopic observations of cell
569 division in *Mycobacterium vaccae* V1. *J Gen Microbiol* 129:2315–2320.
- 570 82. Dahl JL. 2004. Electron microscopy analysis of *Mycobacterium tuberculosis* cell division. *FEMS*
571 *Microbiology Letters* 240:15–20.

- 572 83. Typas A, Banzhaf M, Gross CA, Vollmer W. 2011. From the regulation of peptidoglycan synthesis to
573 bacterial growth and morphology. *Nat Rev Microbiol* 10:123–136.
- 574 84. Zhou X, Halladin DK, Theriot JA. 2016. Fast Mechanically Driven Daughter Cell Separation Is
575 Widespread in Actinobacteria. *mBio* 7:e00952-16.
- 576 85. Zhou X, Halladin DK, Rojas ER, Koslover EF, Lee TK, Huang KC, Theriot JA. 2015. Mechanical crack
577 propagation drives millisecond daughter cell separation in *Staphylococcus aureus*. *Science*
578 348:574–578.
- 579 86. Odermatt PD, Hannebelle MTM, Eskandarian HA, Nievergelt AP, McKinney JD, Fantner GE. 2019.
580 Overlapping and essential roles for molecular and mechanical mechanisms in mycobacterial cell
581 division. *Nature Physics* 16:57-62.
- 582 87. Dufrêne YF. 2020. Together We Are Stronger: Protein Clustering at the Nanoscale. *ACS Nano*
583 14:2561–2564.
- 584 88. Viljoen A, Mignolet J, Viela F, Mathélié-Guinlet M, Dufrêne YF. 2020. How Microbes Use Force To
585 Control Adhesion. *Journal of Bacteriology* 202:e00125-20.
- 586 89. Heath GR, Scheuring S. 2018. High-speed AFM height spectroscopy reveals μ s-dynamics of
587 unlabeled biomolecules. *Nat Commun* 9:4983.
- 588 90. Meister A, Gabi M, Behr P, Studer P, Vörös J, Niedermann P, Bitterli J, Polesel-Maris J, Liley M,
589 Heinzlmann H, Zambelli T. 2009. FluidFM: Combining Atomic Force Microscopy and Nanofluidics
590 in a Universal Liquid Delivery System for Single Cell Applications and Beyond. *Nano Lett* 9:2501–
591 2507.

- 592 91. Guillaume-Gentil O, Potthoff E, Ossola D, Franz CM, Zambelli T, Vorholt JA. 2014. Force-controlled
593 manipulation of single cells: from AFM to FluidFM. *Trends in Biotechnology* 32:381–388.
- 594 92. Guillaume-Gentil O, Mittelviehhaus M, Dorwling-Carter L, Zambelli T, Vorholt JA. 2018. FluidFM
595 Applications in Single-Cell Biology, p. 325–354. *In* *Open-Space Microfluidics*. John Wiley & Sons,
596 Ltd.
- 597
- 598

599 **Figure 1.**

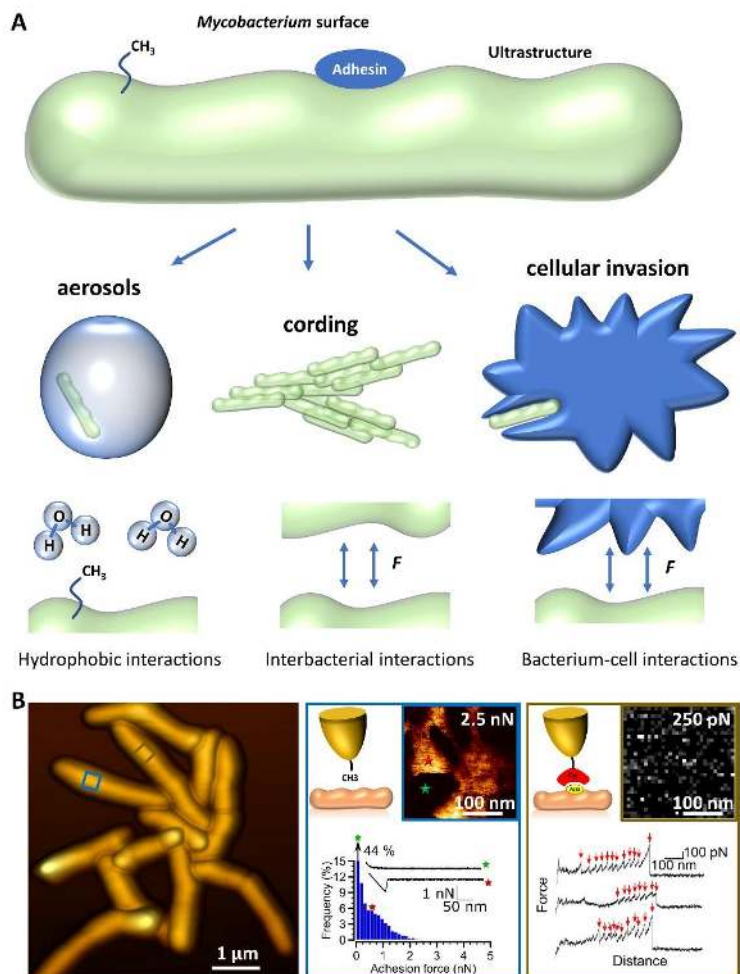
600

601

602 **Fig 1 Two different basic AFM modes to study mycobacterial cells.** (A) AFM imaging, in which the AFM
 603 probe is raster scanned across the sample, allows studying the nanoscale topography and
 604 nanomechanics of cell walls along with correlative fluorescence microscopy imaging of cellular
 605 processes (e.g. markers of cellular division as illustrated by the red-fluorescent beads inside the
 606 bacterium). (B) Force spectroscopy measurements with chemically (e.g. hydrophobic groups such as
 607 saturated acyl chains) or biologically sensitive (e.g. the ligand of an adhesin such as human fibronectin)
 608 tips allows characterization of local hydrophobic properties, and of the strength of adhesin-ligand
 609 complexes.

610

611

612 **Figure 2.**

613

614

615 **Fig 2 The mycobacterial surface at the interface of interactions between bacterial cells and their**616 **environment.** (A) Mycobacteria rely on hydrophobic properties of their surfaces to associate with

617 aerosol droplets and to adhere to each other and form cords. Specialized adhesins stimulate

618 mycobacterium-mycobacterium interactions as well as adhesion of mycobacteria to extracellular matrix

619 proteins and cells. (B) Using AFM force spectroscopy to probe mycobacterial chemical properties and

620 adhesin interactions. Left panel. A 3-D projection of a height image showing a microcolony of

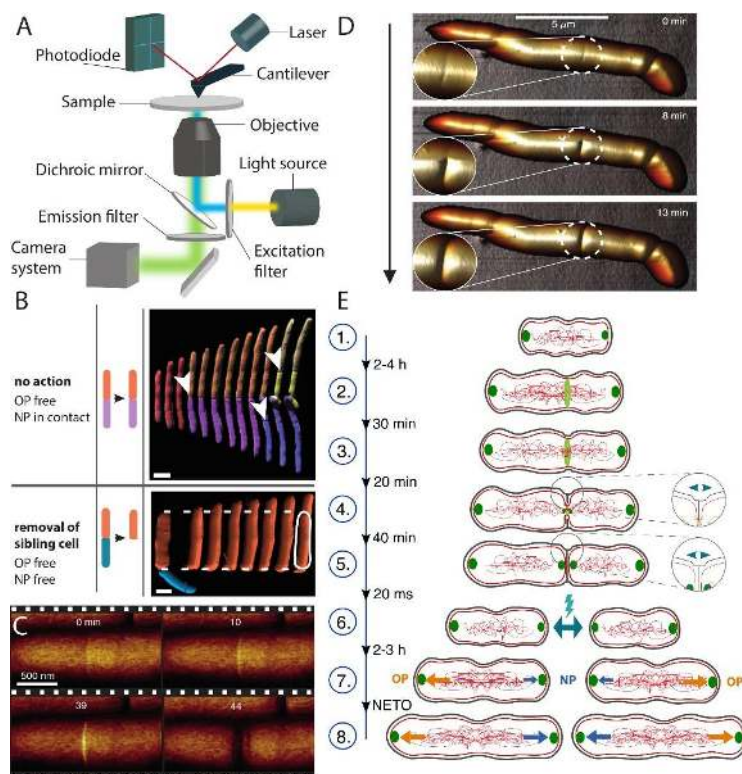
32

621 *Mycobacterium abscessus* cells. Middle panel. AFM probes exposing hydrophobic methyl groups have
622 unraveled hydrophobic properties of mycobacterial cells (top left). Striking hydrophobic (lighter yellow,
623 maximum of 2.5 nN) and hydrophilic nanodomains (darker brown, minimum of 0 nN) were seen on very
624 high-resolution adhesion maps recorded on the surfaces of *M. abscessus* smooth variant
625 (glycopeptidolipid*) cells (top left). On the bottom is shown typical force-distance curves obtained as
626 well as the histogram plots of the frequency distributions of hydrophobic adhesion forces. The red star is
627 indicative of when hydrophobic adhesive forces were registered whereas the green star indicates when
628 no hydrophobic adhesive forces were registered. Adapted with permission from (61). Right panel. AFM
629 probe exposing single molecules of the host extracellular matrix protein, fibronectin (Fn), to which
630 mycobacterial Antigen85 (Ag85, yellow oval) binds. The adhesion map in the top right corner shows a
631 homogenous distribution of Ag85 on the surface of a *M. abscessus* cell. The white pixels represent single
632 adhesins, with the lightest shade representing a maximum adhesion strength of 250 pN and the darkest
633 pixels representing zero adhesion force. Typical force-distance curves of this specific receptor-ligand
634 interaction is shown at the bottom. The sawtooth unbinding peaks relates to sequential unfolding of
635 repeat domains in Fn. Adapted with permission from (48).

636

637 **Figure 3**

638



639

640

641 **Fig 3 Studying cell growth dynamics with correlative AFM-optical microscope.** (A) Schematic
 642 representation of a correlative AFM-optical microscope. The field of view of an inverted fluorescent
 643 microscope is aligned with the cantilever of an AFM in order to acquire correlated images. (B) AFM used
 644 as a nanomanipulation tool. Schematics and time-lapse AFM of growing mycobacteria. Top: Sibling cells
 645 are kept in their original position after cell division. Poles of mother and daughter cells are in close
 646 contact. Bottom: The AFM cantilever was used to remove one of the sibling cells to avoid physical
 647 constraints on the new pole. Adapted from (77) with permission of the author. (C) AFM used for force
 648 spectroscopy. Stiffness measurement of cell surface at the division site between the emergence of the

34

649 pre-cleavage furrow (PCF) and cleavage. Lighter colors represent a higher stiffness. (D) AFM used for
650 topographic imaging. Three-dimensional rendered AFM images of *Mycobacterium smegmatis* before cell
651 cleavage and enlargements of the area around pre-cleavage furrow. The arrow indicates the scan
652 direction. (C)-(D) Adapted from (86) with permission of the author. (E) Schematic representation of the
653 consecutive events leading to cell division in *Mycobacterium smegmatis* studied by correlative AFM-
654 optical microscopy. (1) At cell birth (division of the mother cell), Wag31-GFP (dark green) is localized
655 only at the poles. The cell surface comprises wavelike morphological features, and the subsequent cell
656 division occurs at the center-most trough near mid-cell. (2) FtsZ-GFP (light green) localizes at the central
657 wave trough and forms a circumferential ring. (3) Formation of the pre-cleavage furrow starts, which is
658 co-localized with the FtsZ-ring. (4) Stress builds up, whereas membrane strength decreases at pre-
659 cleavage furrow. Septum formation and cytokinesis occur. Wag31-GFP localizes to the future division
660 side, whereas the FtsZ-ring disassembles. (5) The tensile stress increases. (6) Further increase of turgor
661 pressure cumulates in physical cell separation by rapid mechanical rupture leading to newborn sibling
662 cells. (The space between the sibling cells after division was inserted for visualization purposes. In
663 reality, the sibling cells stay in proximity to each other) (7) Pre-“new end take off” (NETO) phase: Slow
664 growth rate of the new pole (NP). Reallocation of Wag31 from the old pole (OP) to the new pole. (8)
665 Post-NETO phase: Growth-rate change (NETO) is followed by a fast growth rate of the new poles. The
666 old poles grow in both phases with a constant, fast rate.

667

